Am J Cancer Res 2024;14(4):1594-1608
www.ajcr.us /ISSN:2156-6976/ajcr0154780

Original Article

Mesenchymal stem cells derived from adipose tissue and umbilical cord reveal comparable efficacy upon radiation-induced colorectal fibrosis in rats

Mya Thandar[1,2], Xiaojie Yang[2,6], Yuanchang Zhu[1,2], Ying Huang[1,3], Xueying Zhang[1,2], Shenghui Huang[1,3], Leisheng Zhang[4,5], Pan Chi[1,2,3]

[1]Department of Colorectal Surgery, Fujian Medical University Union Hospital, Fuzhou 350001, Fujian, China; [2]Key Laboratory of Ministry of Education for Gastrointestinal Cancer, Department of Colorectal Surgery, Fujian Medical University, Fuzhou 350001, Fujian, China; [3]Training Center of Minimally Invasive Surgery, Fujian Medical University Union Hospital, Fuzhou 350001, Fujian, China; [4]Science and Technology Innovation Center, The Fourth People's Hospital of Jinan (The Third Affiliated Hospital of Shandong First Medical University), Jinan 250031, Shandong, China; [5]National Health Commission (NHC) Key Laboratory of Diagnosis and Therapy of Gastrointestinal Tumor, Gansu Provincial Hospital, Lanzhou 730000, Gansu, China; [6]Department of Thoracic Surgery, The Third Affiliated Hospital of Chongqing Medical University, Chongqing 401100, China

Received December 5, 2023; Accepted February 2, 2024; Epub April 15, 2024; Published April 30, 2024

Abstract: Chemoradiotherapy (CRT) and radiotherapy (RT) have served as anticancer treatments and neoadjuvant therapies for conquering multimodal rectal cancers including colorectal carcinoma (CRC), yet the concomitant radiation-induced colorectal fibrosis (RICF) has caused chronic toxicity and stenosis in the colorectal mucosa of patients. Mesenchymal stem/stromal cells (MSCs) with unique bidirectional immunoregulation and anti-fibrotic effect have been recognized as splendid sources for regenerative purposes including intestinal diseases. Herein, we are aiming to verify the feasibility and variations of MSC-based cytotherapy for the remission of RICF from the pathological features and the potential impact upon the transcriptomic signatures of RICF rats. For the purpose, we utilized our well-established RICF Sprague-Dawley (SD) rats by radiation for five weeks, and conducted consecutive intraperitoneal injection of two distinct MSCs for treatment, including MSCs derived from adult adipose tissue (AD-MSCs) and perinatal umbilical cord (UC-MSCs). On the one hand, the efficacy of AD-MSCs and UC-MSCs was assessed by diverse indicators, including weight change, pathological detections (e.g., H&E staining, Masson staining, EVG staining, IF staining, and IHC staining), and proinflammatory and fibrotic factor expression. On the other hand, we turned to RNA-sequencing (RNA-SEQ) and multifaceted bioinformatics analyses (e.g., GOBP, Venn Map, KEGG, and GSEA) to compare the impact of AD-MSC and UC-MSC treatment upon the gene expression profiling and genetic variations. RICF rats after consecutive AD-MSC and UC-MSC administration revealed comparable remission in histopathogenic features and significant suppression of diverse proinflammatory and fibrotic factors expression. Meanwhile, RICF rats after both MSC treatment revealed decrease and variations in the alterations in diverse gene expression and somatic mutations compared to RICF rats. Collectively, our data indicated the comparable therapeutic effect of AD-MSCs and UC-MSCs upon RICF in SD rats, together with the conservations in gene expression profiling and the diverse variations in genetic mutations. Our findings indicated the multifaceted impact of MSC infusion for the supervision of RICF both at the therapeutic and transcriptomic levels, which would provide novel references for the further evaluation and development of MSC-based regimens in future.

Keywords: Radiation-induced colorectal fibrosis (RICF), mesenchymal stem/stromal cells (MSCs), pathological features, transcriptomic signatures, anti-fibrotic effect

Introduction

Radiation-induced colorectal fibrosis (RICF) is a persistent adverse outcome observed following pelvic radiation for colorectal cancer [1, 2]. This condition prolongs the recovery period for surgical anastomosis, resulting in complications such as anastomotic leakage, stenosis, and an increased susceptibility to post-cancer surgery issues (e.g., rectovaginal fistula, recto-

https://doi.org/10.62347/DRAE5818

vesical fistula, and bowel obstruction) [3-5]. These complications significantly impact the overall quality of life of patients with colorectal cancer and the concomitant RICF. Despite efforts with available medications proving suboptimal in preventing and addressing RICF, endoscopic or surgical interventions remain the primary options for managing the symptomatic intestinal strictures [6, 7]. Therefore, there is a booming need to further explore effective treatment options for RICF.

Stem cells are unique cell populations with self-renewal and multi-lineage differentiation potential, which thus supply therapeutic alternatives for diverse intractable diseases and tissue rejuvenation [8, 9]. Of them, mesenchymal stem/stromal cells (MSCs) are non-hematopoietic cells with splendid bidirectional immunoregulatory capacity and versatile differentiation potential, which thus have been recognized as promising candidates for regenerative medicine [10, 11]. For decades, we and other investigators have identified MSCs from diverse tissues and even derived from pluripotent stem cells [10-12]. Of them, adipose tissue serves as a convenient, abundant, and easily accessible source of MSCs, with a harvest procedure that is comparatively less invasive than other alternatives [13, 14]. Instead, human umbilical cord tissue serves as another resource with robust *ex vivo* proliferative capacity for MSC-based therapies [10]. Notably, considerable literatures indicate that MSCs derived from umbilical cord tissue exhibit a more primitive, proliferative, and immunosuppressive profile compared to their adult counterparts [15-18]. However, the therapeutic effect and the potential omics impact of MSCs derived from adult adipose tissues (AD-MSCs) and perinatal umbilical cord (UC-MSCs) upon radiation-induced colorectal fibrosis (RICF) are largely obscure.

Therewith, in this study, we are aiming to compare the potential efficacy of adult AD-MSCs and perinatal UC-MSCs upon an experimental model of colorectal fibrosis induced by radiation from the aspects of *in vivo* biofunction and transcriptomics. For the purpose, we took advantage of our-well-established RICF rat model [1, 2], and conducted consecutive intraperitoneal injection of AD-MSCs and UC-MSCs to verify the potential impact upon the pathological and transcriptomic signatures of colorectal tissues in RICF rats. With the aid of multifaceted biological analyses, we verified that AD-MSCs and UC-MSCs revealed comparable alleviative effect upon the pathological features of RICF rats. Meanwhile, RICF rats after both MSC administration showed considerable conservations and alterations in gene expression pattern and somatic variations. Collectively, our data indicated the application of both AD-MSCs and UC-MSCs for RICF treatment, together with the systematic and detailed information upon the transcriptomic features of colorectal tissues in RICF rats, which would benefit the further development of MSC-based cytotherapy in preclinical and clinical investigations.

Materials and methods

Cell culture

Human adipose tissue-derived MSCs (AD-MSCs) and umbilical cord-derived MSCs (UC-MSCs) at passages 3-8 were purchased from Shanghai HonSun Biological Technology Co., Ltd. (China) and H&B Biotech Co., Ltd. respectively (China). The AD-MSCs and UC-MSCs were cultured in DMEM basal medium supplemented with 10% FBS (Australia), 1% penicillin and streptomycin (ThermoFisher, USA). For cell passage, AD-MSCs and UC-MSCs were dissected with 0.25% Trypsin/EDTA (Gibco, USA) for 5 min, and then enriched by centrifugation at 300×g at room temperature (RT). After resuspension, AD-MSCs and UC-MSCs were seeded in the aforementioned MSC culture medium at 37°C, 5% CO_2.

Procurement and housing of experimental animals

Male Sprague-Dawley (SD) rats, aged 6-8 weeks and weighing 300-350 g, were purchased from the Laboratory Animal Center of Fujian Medical University. The rats were maintained on a standard chow diet with unrestricted access to water, housed at a temperature of 23 ± 3°C, and subjected to a 12-hour light/dark cycle. Ethical clearance for all experimental protocols was obtained from the Institutional Animal Care and Use Committee of Fujian Medical University (approval No.: FJMU IACUC 2021-0510), adhering to the International Guiding Principles for Biomedical Research Involving Animals.

Experimental design and animal grouping

The SD rats were randomly divided into four groups, including the control healthy group (Ctr), the radiation-induced colorectal fibrosis group (RICF) (4 Gy per minute for a cumulative dose of 20 Gy), and the RICF rats with either AD-MSC (AD-MSC) or UC-MSC (UC-MSC) treatment. Anesthesia was induced via intraperitoneal injection of 10% chloral hydrate (3 ml per kilogram body weight). RICF rats in the AD-MSC and UC-MSC groups underwent intraperitoneal injections of 1×10^6 AD-MSCs and UC-MSCs twice a week for a duration of five weeks since the fifth week post-irradiation. Daily monitoring of the rats' physical condition were conducted, including abdominal distension, diarrhea or bloody stools, depilation on the area of irradiation, and weekly recording of body.

Experimental endpoint and tissue handling

All rats were sacrificed in the tenth week post-irradiation. Histopathological examination was performed on three 5 mm segments of the rectum, located 1 cm proximal to the anus, which were excised and fixed in 10% formalin (Sigma-Aldrich, USA). The remaining tissue samples were immediately frozen in liquid nitrogen and turned to wash with 1×PBS (Solarbio, China) for subsequent analyses.

Histological evaluation

In order to evaluate the histological features of intestinal tissue, 5 μm thick sections were prepared and subsequently subjected to hematoxylin and eosin (H&E) staining, Masson's trichrome staining, and Verhoeff Van Gieson (EVG) staining (Elastic stain kit, Abcam, UK) according to the manufacturer's instructions. The assessment of radiation-induced injury was conducted based on radiation injury score (RIS) as reported by Langberg *et al* [19]. For quantitative analysis, the submucosal thickness was measured at five randomly selected points of each sample, while the depth of the submucosa was determined by calculating the distance between the muscularis mucosae and muscularis propria. Morphometric analysis, carried out under a 400× magnification, involved two pathologists independently assessing five different fields to ensure comprehensive evaluation.

Immunohistochemical (IHC) analysis

Tissue sections (5 μm) from distinct groups (Ctr, RICF, AD-MSC, and UC-MSC) underwent deparaffinization in xylene and subsequent rehydration through a graded series of ethanol solutions. After rinsing in tap water and distilled water, antigen retrieval was achieved by subjecting tissue slides to a 1× citrate antigen retrieval solution, boiling for 15 minutes, and washing with 1×PBS for three times after cooling to RT. To quench endogenous peroxide activity, tissue sections were incubated in an endogenous peroxide blocking solution for 30 min, followed by blocking with normal goat serum for 20 min at 37°C. Subsequently, sections were incubated overnight at 4°C with specific primary antibodies (anti-collagen I, anti-α-SMA, anti-fibronectin antibody). This was succeeded by incubation with goat anti-rabbit IgG H&L/Biotin antibody at 37°C for 20 min, followed by streptavidin/HRP incubation. The colorectal tissue sections were then exposed to DAB substrate for 5 min and counterstained with hematoxylin for 3 min. Imaging of the sections was accomplished using a Digital Pathological Scanner (Leica Aperio CT6, Germany). Detailed information regarding the utilized antibodies is available in Table S1.

Immunofluorescence (IF) staining

IF staining was conducted as we previously described with several modifications [11, 20]. In details, tissue sections were incubated with primary antibodies (anti-collagen-1, anti-α-SMA, anti-fibronectin) overnight at 4°C in dark, and following by incubation with the corresponding secondary antibodies (goat anti-rabbit IgG, goat anti-mouse IgG) for 1 hr at RT and with DAPI for 10 min in dark. The sections were then washed with 1×PBS and subjected to examination using a confocal laser scanning microscope (Leica SP5, Germany). Detailed information regarding the utilized antibodies is available in Table S2.

Quantitative real-time polymerase chain reaction (qRT-PCR)

Total RNAs in colorectal tissues of the indicated SD rats were extracted using TRIzol reagent (GK20008, GLPBIO) according to the manufacturer's instructions. After that, cDNAs were synthesized by utilizing the HiScript® III RT SuperMix

for qPCR (+gDNA wiper) (R323-01, Vazyme). Then, qRT-PCR analysis was performed with the Taq Pro Universal SYBR qPCR Master Mix (Q712, Vazyme). The mRNA expression levels of target genes were quantified by utilizing the standard $2^{-\Delta\Delta Ct}$ method as we reported before [12, 21]. The list of the primer sequences is available in Table S3.

Western-blotting analysis

Total proteins were extracted from cryopreserved colorectal tissues using RIPA lysis buffer (PC101, Epizyme), and the concentration was determined with the Enhanced BCA Protein Assay Kit (ThermoFisher Scientific, USA). Then, total proteins were turned to SDS-PAGE-based electrophoresis and PVDF-based transmembrane (0.45 μm, IPVH00010, Immobilon®-P, Millipore). After a 20-30 min incubation in blocking buffer (PS108P, Epizyme), the membranes were probed overnight with specific primary antibodies (anti-CTGF, anti-α-SMA, anti-TGF-β1, anti-Vimentin, anti-p-SMAD2/3, anti-MMP-2, anti-MMP-9, anti-Collagen-1, anti-Fibronectin, anti-GAPDH). After that, the membranes were incubated with the corresponding secondary antibodies (Goat Anti-Rabbit IgG, Goat Anti-Mouse IgG) for 2 hrs and followed by exposure with ImageQuant™ LAS 4000 mini. Finally, quantitative analysis was conducted with Image J software (version 1.53k) as we described before [9, 11]. The detailed information of the indicated antibodies is available in Table S4.

RNA-sequencing (RNA-SEQ) and bioinformatics analysis

RNA-SEQ and multifaceted bioinformatics analyses were performed as we recently reported [22, 23]. In details, a total number of 12 RNA samples were harvested from the colorectal tissues of the indicated SD rats in the indicated groups, including the control group (C1, C2, C3), the RICF group (R1, R2, R3), the RICF rats with AD-MSC treatment (A1, A2, A3) group, and the RICF rats with UC-MSC treatment (U1, U2, U3) group. Then, the RNAs were turned to BGI Genomics (Shenzhen, China) for RNA-SEQ analysis. All bioinformatics analyses were conducted by utilizing the online platforms, including HeatMap, scatter plot, principal component analysis (PCA), gene set enrichment analysis (GSEA), gene ontology biological process (GOBP), and Kyoto Encyclopedia of Genes and Genomes (KEGG). The list of the differentially expressed genes (DEGs) between the indicated groups is available in Table S5.

Statistical analysis

The statistical analyses were conducted using Graph Pad Prism 9.1.1 (223) (©1994-2021 GraphPad Software, LLC.). In brief, comparisons between two unpaired groups were performed using the student's unpaired T-test, while the one-way ANOVA test was employed to analyze data among multiple unpaired groups. Results are presented as mean ± SD based on three independent experiments, and statistical significance was considered at a *P* value less than 0.05 ($P < 0.05$). ns, not significant; *, $P < 0.05$; **, $P < 0.01$; ***, $P < 0.001$; ****, $P < 0.0001$.

Results

AD-MSCs and UC-MSCs showed comparable alleviative effect upon the pathological manifestations in RICF rats

RICF rat models were constructed as we recently reported [1, 2], and consecutive intraperitoneal injection of AD-MSCs or UC-MSCs was performed since the 5th week to the 10th week. Compared with the control healthy group (denoted as C), rats in RICF group (denoted as R) showed intestinal strictures in the irradiated segments at the 10th week. Instead, the colorectal area of RICF rats with AD-MSC or UC-MSC treatment (denoted as A and U, respectively) revealed significant remission and comparable morphological structure as in RICF rats (**Figure 1A**). According to the mean live weight of the rats, a gradual body weight loss was observed in the RICF group when compared with the Ctr group ($P < 0.0001$), which was consistently alleviated by both MSC treatment (**Figure 1B**).

As shown in **Figure 1C**, the multifaceted pathological changes in RICF rats, including fibrotic lesion, collagen deposition and elastic fibers, were sharply decreased after AD-MSCs or UC-MSCs administration according to H&E staining, Masson staining and EVG staining of the colorectal tissues. On the basis of radiation injury score (RIS), we noticed the incrassated submucosa of the colorectum in the RICF group

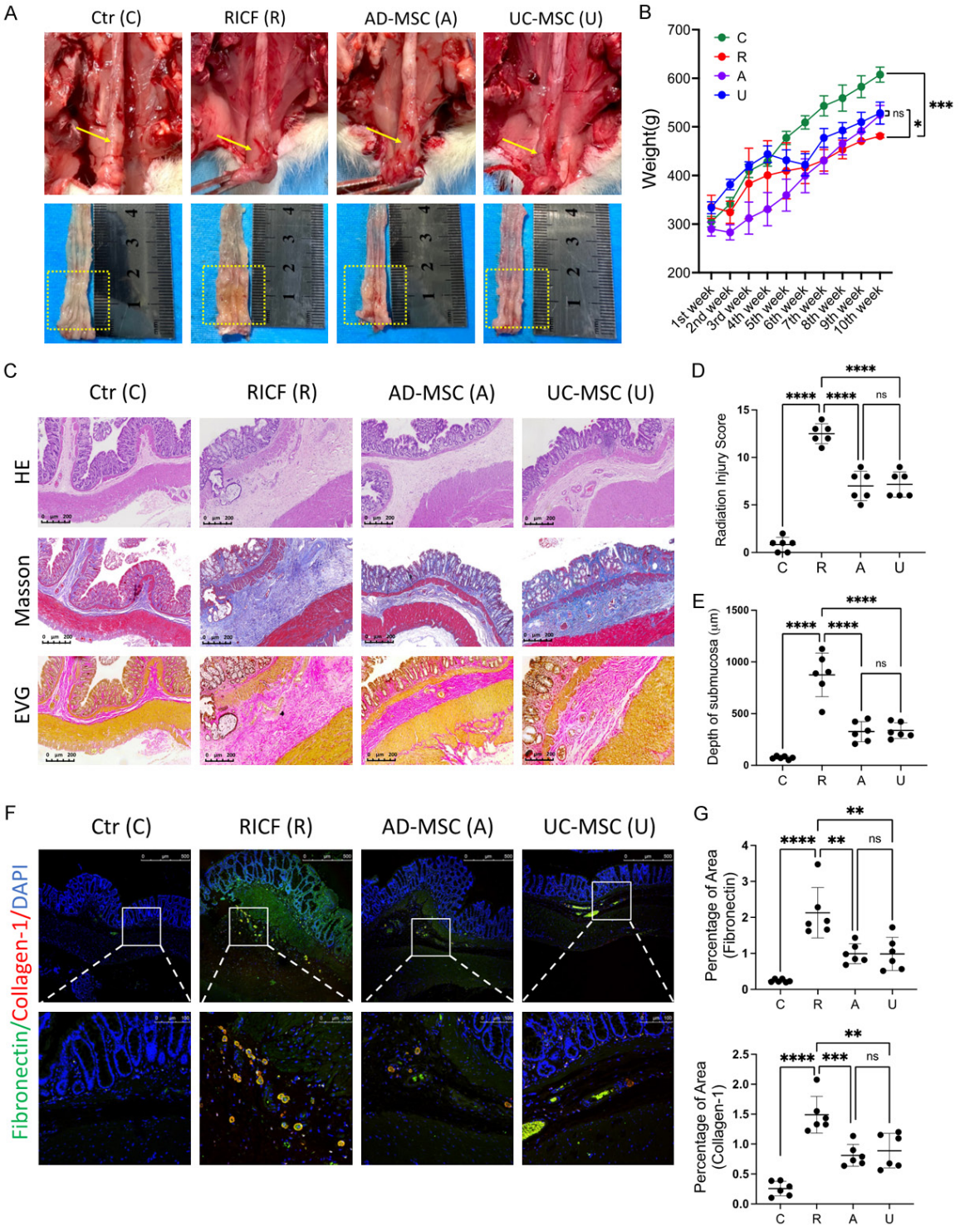

Figure 1. Comparison of the ameliorative effect of AD-MSCs and UC-MSCs upon the manifestation of RICF in SD rats. (A) Representative macroscopic features of the colorectal tissues of SD rats at the 10th week in the control group (Ctr), the radiation-induced RICF group (RICF), the AD-MSC-treated RICF group (AD-MSC), and the UC-MSC-treated RICF group (UC-MSC). (B) Dynamic body weight variations of SD rats in the indicated groups within 10 weeks. (C) Representative photomicrographs of colorectal tissues with HE staining (upper panel), Masson's trichrome staining (middle panel), and EVG staining (bottom panel) in the aforementioned groups. Scale bar = 200 μm. (D) Comparison of histological radiation injury score of colorectal tissues in the indicated groups. (E) Statistical analysis of the depth of submucosal layer in the indicated groups. (F, G) Representative immunofluorescent images (F) and statistical analyses of the percentages of indicated areas (G) with Fibronectin and Collagen-1 expression in colorectal tissues of SD rats in the indicated groups. Scale bar = 500 μm (upper panel), Scale bar = 100 μm (lower panel). Data are presented as mean ± SD (n = 6). ns, not significant; *P < 0.05, **P < 0.01, ***P < 0.001, ****P < 0.0001.

(RICF vs. Ctr = 12.5 ± 1.05 vs. 0.83 ± 0.75, P < 0.001) was moderately relieved in the AD-MSC (AD-MSC vs. RICF = 7.00 ± 1.55 vs. 12.33 ± 1.16, P < 0.001) and UC-MSC groups (UC-MSC vs. RICF = 7.17 ± 1.33 vs. 12.33 ± 1.16, P < 0.001) (**Figure 1D**). In consistence, the increased depth of submucosa in the RICF group was significantly suppressed in the AD-MSC and UC-MSC group, respectively (**Figure 1E**). Furthermore, with the aid of immunofluorescent staining (IF) and statistical analysis, we intuitively observed the sharp decline in the percentage of areas with Fibronectin and Collagen-1 co-expression in RICF rats by continuous AD-MSC and UC-MSC treatment (**Figure 1F**, **1G**). Taken together, these data indicated the comparable ameliorative effect of AD-MSC and UC-MSC upon the pathological lesions of colorectal tissues in RICF rats.

RICF rats revealed consistent remission in fibrosis and inflammatory response after AD-MSCs and UC-MSCs treatment

To further evaluate the therapeutic effect of AD-MSC and UC-MSC, we incipiently turned to compare the anti-fibrotic efficacy upon the colorectal tissue of RICF rats. As shown by the immunohistochemical staining (IHC) and qRT-PCR analysis, RICF rats exhibited high level expression of fibrosis-related genes (Collagen-1, Collagen-3, Fibronectin, α-SMA, TIMP-1, SERPINE-1), which could be significantly suppressed by continuous AD-MSC and UC-MSC infusion (P < 0.001) (**Figure 2A**, **2B**). Meanwhile, we noticed the hyperactivation of inflammatory response in the colorectal tissues of RICF rats was indiscriminatingly alleviated in the AD-MSC and UC-MSC groups according to proinflammatory factor expression (TGF-β1, IL-6, IL-1β) (**Figure 2C**). However, there was no statistical significance between the indicated groups on other pro-inflammatory factors such as IL-12, TNF-α and IL-17. In consistence, by conducting western-blotting analysis and statistical analysis, we observed the moderate decline in the protein expression of fibrosis-related genes (Fibronectin, Collagen-1, Vimentin, CTGF) and proinflammatory factors (TGF-β1, p-Smad2/3), together with matrix metalloproteinase (MMP-2, MMP-9) (**Figure 2D**, **2E**). Collectively, these finding revealed that AD-MSCs and UC-MSCs revealed comparable anti-fibrotic effect and anti-inflammatory response in RICF rats.

The multifaceted signatures of gene expression profiling in RICF rats after AD-MSC and UC-MSC treatment

Having illuminated the therapeutic effect upon RICF, we next tried to explore the impact of AD-MSCs and UC-MSCs upon the gene expression pattern of colorectal tissues. For the purpose, we took advantage of RNA-SEQ and multifaceted bioinformatics analyses, and found that rats in all groups revealed conservations in general gene expression profiling based on TPM (transcripts per kilobase million) values and FPKM (fragments per kilobase million) values of individual genes (**Figure 3A**, **3B**). From the viewport of principal component analysis (PCA) and Pearson correlation, we could intuitively observed the distinctions between the RICF group and the relative groups, which indicated the alterations in the affinity and gene expression in RICF rats (**Figure 3C**, **3D**).

Furthermore, with the aid of scatter plot diagram and bar chart, the distribution of the differently expressed genes (DEGs) and the relative genes (no-DEGs) between the indicated groups could be intuitively observed (**Figure 3E**, **3F**). For instance, Mmp7 and Spink3 were significantly upregulated and downregulated in the colorectal tissues of RICF rats compared to the Ctr group (R vs. C), whereas the expression pattern of these two representative genes was reversed after AD-MSC treatment (A vs. R) (**Figure 3E**). Differ from those with numerous DEGs between the RICF group and the relative groups, there were minimal DEGs among the Ctr, AD-MSC and UC-MSC groups, which collectively indicated the therapeutic effect of the aforementioned MSCs upon RICF rats (**Figure 3F**). With the aid of Venn Map diagram, we could clearly observe the distribution of the number of gene expression among the indicated groups. For example, we noticed a total number of 17154 overlapped genes were expressed in all groups, whereas only 331 genes were specifically expressed in RICF rats (**Figure 3G**). Additionally, according to the HeatMap diagram of DEGs, we could find the distant hierarchical clustering relationship between the RICF group and the relative groups (**Figure 3H**). Taken together, these data exhibited the multifaceted similarities and differences in the gene expression profiling among the indicated group, and colorectal tissues of RICF rats

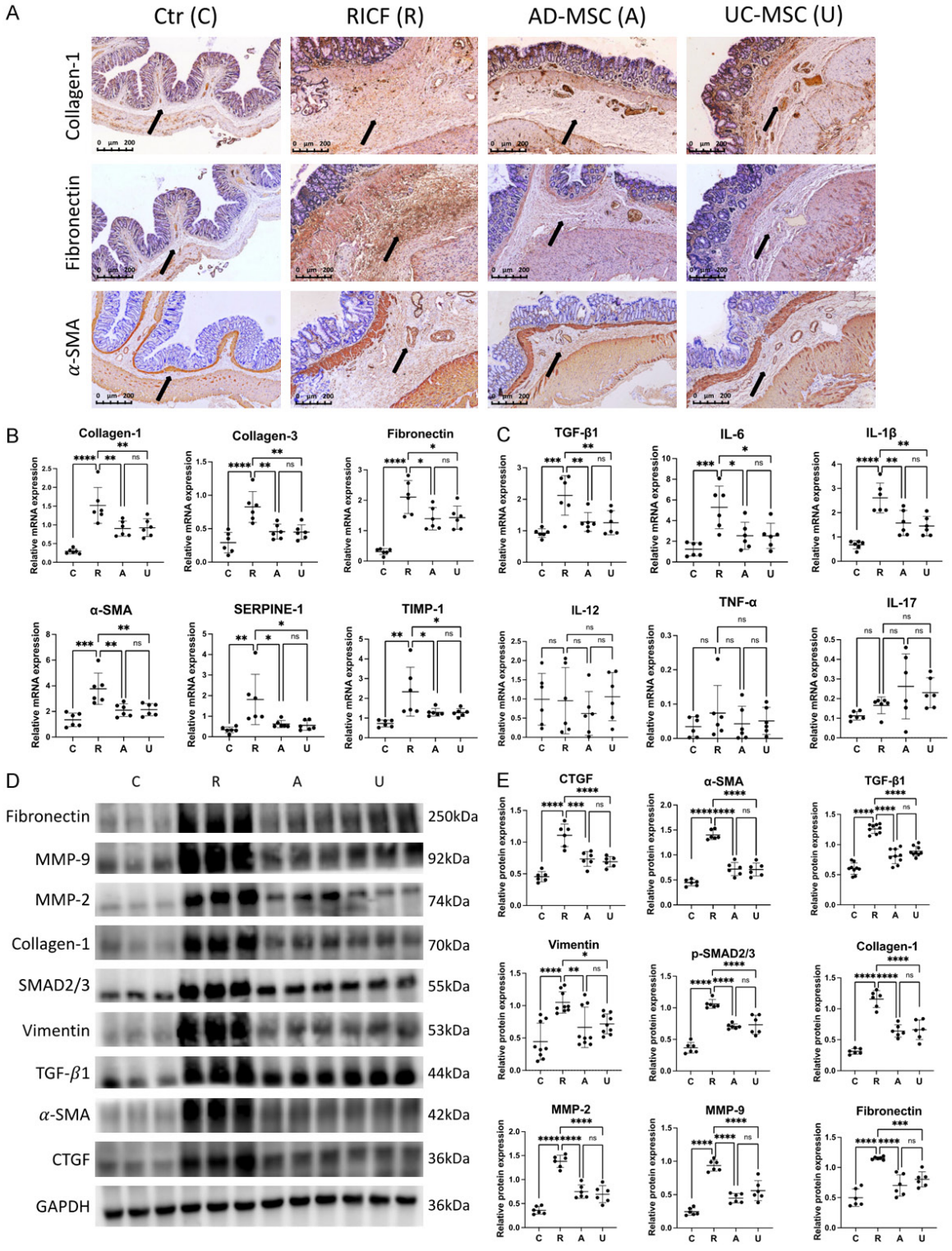

Figure 2. The anti-fibrotic effects and anti-inflammatory effects of AD-MSC and UC-MSC upon RICF in SD rats. (A) Representative immunohistochemical (IHC) images of colorectal tissues with Collagen-1, Fibronectin, and α-SMA expression in the indicated groups. Scale bar = 200 μm. (B, C) qRT-PCR analysis of mRNA expression of the indicated genes (Collagen-1, Collagen-3, Fibronectin, α-SMA, TIMP-1, SERPINE-1, TGF-β1, IL-6, IL-1β, IL-12, TNF-α, IL-17) in the colorectal tissues of the indicated SD rats. (D, E) Western-blotting bands (D) and quantitative analysis (E) of the indicated genes (CTGF, α-SMA, TGF-β1, Vimentin, p-SMAD2/3, Collagen-1, MMP-2, MMP-9, Fibronectin) at protein level in the aforementioned colorectal tissues. Data are presented as mean ± SD (n = 6). ns, not significant; *P < 0.05, **P < 0.01, ***P < 0.001, ****P < 0.0001.

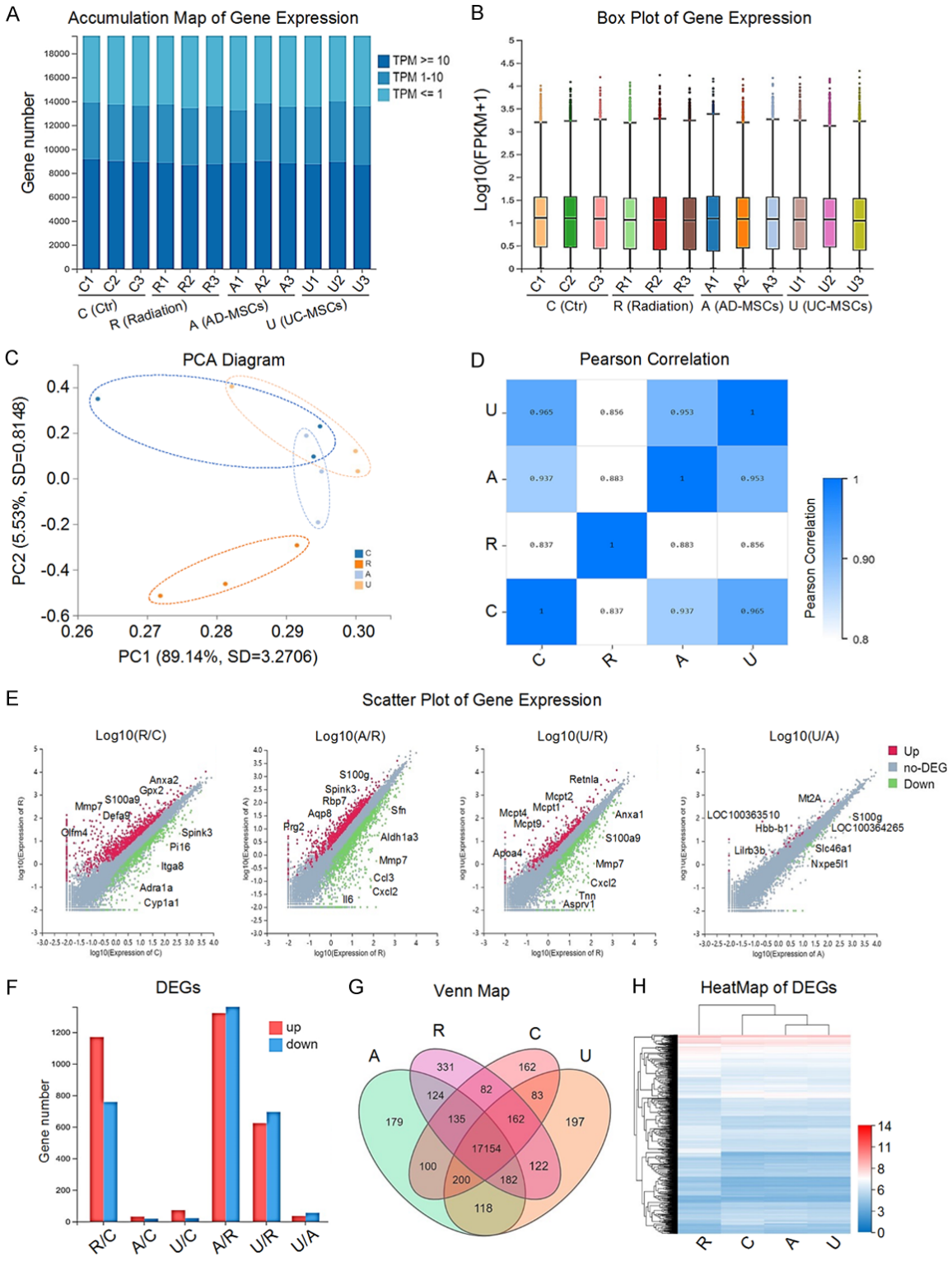

Figure 3. The gene expression profiling of colorectal tissues after AD-MSC and UC-MSC administration. (A, B) The accumulation map (A) and box plot (B) of the overall gene expression in colorectal tissues of SD rats in the indicated groups. (C, D) Principal analysis (PCA) (C) and Pearson correlation (D) showed the affinity of SD rats in the indicated groups. (E) Scatter plot showed the differentially expressed genes (DEGs) and the non-DEGs between the indicated groups. (F) Bar chart diagram showed the upregulated (Up) and downregulated (Down) DEGs between the aforementioned groups. (G) Venn map diagram revealed the distribution of the gene expression pattern among the indicated groups. (H) HeatMap diagram showed the hierarchical clustering relationship of the DEGs between the indicated groups.

revealed distant hierarchical clustering relationship against that in the relative groups.

The biofunction of the DEGs enriched in RICF rats were mainly involved in anti-inflammatory response

To further dissect the biological significances of the enriched DEGs, we conducted gene ontology biological process (GOBP) analysis, and found that the DEGs between the RICF and AD-MSC groups (A vs. R) were mainly involved in diverse inflammatory response and metabolism (e.g., colorectal tissues, cellular response to IL-1, neutrophil chemotaxis, inflammatory response), whereas those between the AD-MSC and UC-MSC groups (U vs. A) were principally involved in diverse processes such as chemokine-mediated signaling pathway and response to metal ion (**Figure 4A**, **4B**). In consistence, representative inflammatory response-associated signaling pathways (e.g., IL-17 signaling pathway, TNF signaling pathway) were enriched by KEGG analysis between the RICF and AD-MSC groups, or between the AD-MSC and UC-MSC groups (**Figure 4C**, **4D**).

Simultaneously, we turned to gene set enrichment analysis (GSEA) and noticed the specific enrichment of the inflammatory response-related gene sets between the RICF and AD-MSC groups, and the cytokine-cytokine interaction-related gene sets between the AD-MSC and UC-MSC groups, respectively (**Figure 4E**). In consistence, the gene sets involved in TNF signaling pathway (A vs. R) and IL-17 signaling pathway (U vs. A) were enriched between the aforementioned groups, respectively (**Figure 4F**). Additionally, the spatial distribution and relationship of the indicated DEGs (KDA, initial genes, and associated genes) among the indicated groups were shown according to the diagram of key drive gene analysis (KDA) (**Figure 4G**). Collectively, these data revealed the principal biofunction of the DEGs among the groups, and in particular, the inflammatory response-associated genes in RICF rats after MSC treatment.

The consistent impact of AD-MSC and UC-MSC treatment upon the genetic variation spectrum of colorectal tissues in RICF rats

To further dissect the impact of AD-MSC and UC-MSC infusion upon the transcriptomic features of colorectal tissues in RICF rats, diverse variable shear events (VSEs) were observed and a similar pattern were observed among all groups, including the as_a3ss, as_a5ss, as_ri, and as_se subsets (**Figure 5A**). As to the differentially VSEs (DVSEs), the as_se subset served as the dominate VSEs between the indicated groups (**Figure 5B**). Interestingly, RICF rats after AD-MSC (A/R) or UC-MSC (U/R) treatment also showed distinct percentages of the as_a3ss and as_a5ss subsets, whereas the A/C and U/A groups exhibited differences in the content of the as_se, as_a5ss and as_mxe subsets of somatic mutations instead (**Figure 5B**). Subsequently, we found there was no clear tendency in genetic relationship among the indicated groups according to the PCA diagram and Pearson correlation analysis (**Figure 5C**, **5D**). Simultaneously, on the basis of Circos diagram, we also didn't observe obvious tendency in the distribution of gene fusion events among all groups (**Figure 5E**). Furthermore, we also dissected the expression pattern of the aforementioned 13 genes with somatic mutations, and found there were minimal differences in the expression pattern but revealed two distinct subsets in hierarchical clustering (**Figure 5F**). By performing protein-protein interaction (PPI) analysis, no obvious interactions were noticed among the 13 genes with somatic mutations (**Figure 5G**). Overall, these data indicated the conservations and diverse variations in the subsets and distribution of somatic mutations in RICF rats after AD-MSC and UC-MSC treatment.

Discussion

Radiation-induced colorectal fibrosis (RICF) has caused pathological lesions to patients and largely limits the dose delivery of radiotherapy for colorectal carcinoma (CRC) [1]. Despite the considerable progress in the supervision of RICF and radiation-induced colorectal damage (RICD) (e.g., pirfenidone, interferon gamma), the outcomes of patients are far from satisfaction and the concomitant untoward effects (e.g., fibrosis, hyperactivated inflammatory response) are still intractable. In this study, we took advantage of our well-established RICF SD rat model for the mimick of the pathological manifestations and the evaluation of the efficacy of adult AD-MSCs and perinatal UC-MSCs. With the aid of multifaceted biological and tran-

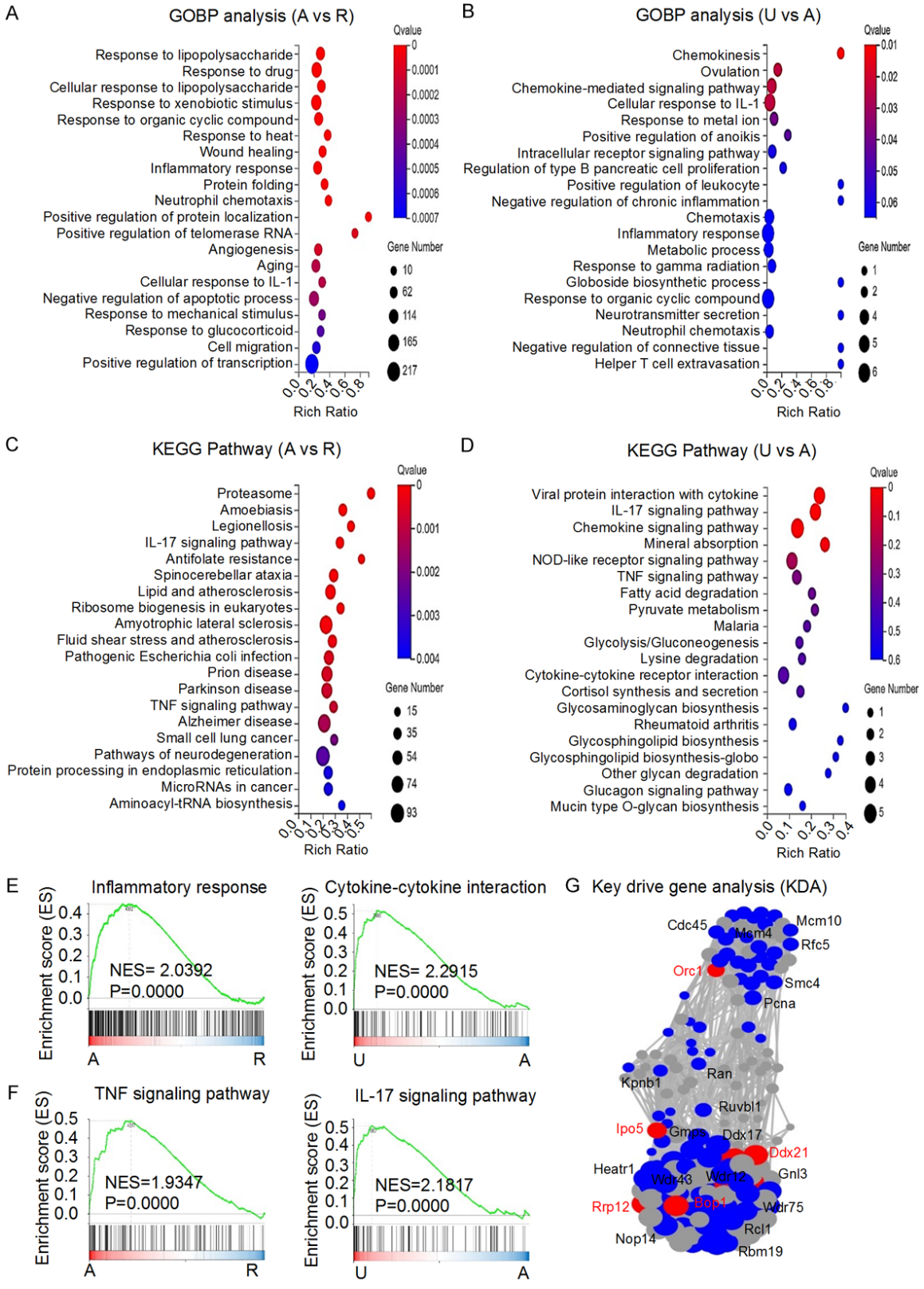

Figure 4. Comparison of the biological process variations of DEGs in RICF rats after AD-MSC and UC-MSC treatment. (A, B) Gene ontology biological process (GOBP) analysis of DEGs between the A and R groups (A), or between the U and A groups (B). (C, D) KEGG signaling pathway analysis of DEGs between the A and R groups (C), or between the U and A groups (D). (E, F) Gene set enrichment analysis (GSEA) revealed the indicated biological processes (E) and signaling pathways (F) between the A and R groups (left panel), or between the U and A groups (right panel). (G)

Key drive gene analysis (KDA) showed the interactions of the indicated genes (associated gene, initial gene, KDR) among the indicated groups.

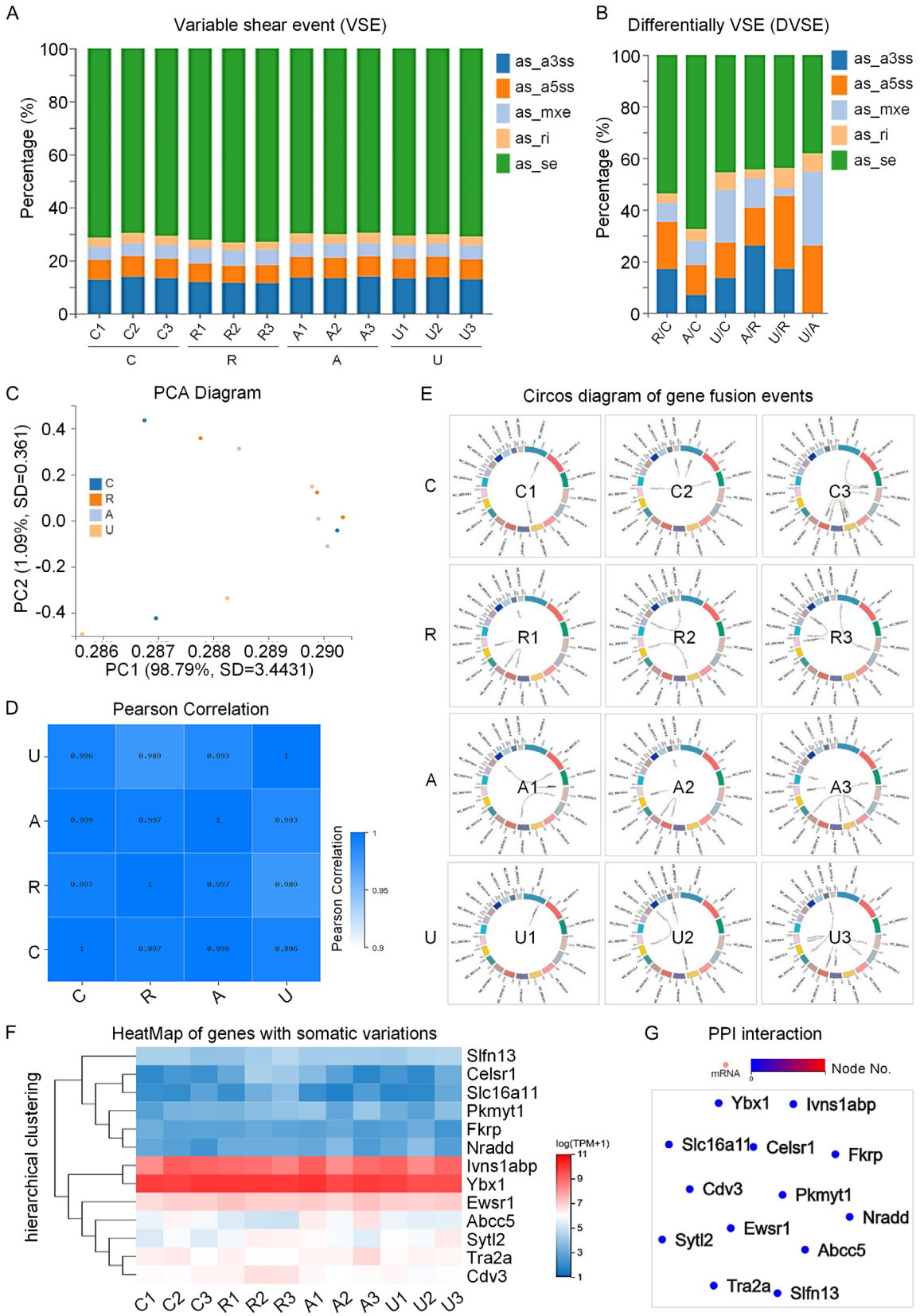

Figure 5. Comparison of the gene spectrum with genetic variations in RICF rats after AD-MSC and UC-MSC treatment. (A, B) Variable shear events (VSE) (A) and the differentially VSE (DVSE) (B) of the gene spectrum in colorectal tissues of SD rats in the groups. (C, D) The PCA diagram (C) and Pearson correlation (D) of the SD rats with genetic mutation and variation spectrum in the indicated groups. (E) Circos diagrams showed the spatial distribution of the gene fusion events in the indicated groups. (F) HeatMap diagram exhibited the hierarchical clustering of the genes with somatic mutations among the indicated groups. (G) Protein-protein interaction (PPI) network showed the potential correlations of the genes with genetic mutations among the indicated groups.

scriptomic analyses, we verified that both AD-MSCs and UC-MSCs revealed comparable therapeutic effect upon RICF rats, but showed diverse impact upon the gene expression profiling and genetic variations.

In the context of treating pelvic malignancies, radiotherapy (RT) is a commonly employed modality, demonstrating effectiveness in many cases. However, the therapeutic benefits are accompanied by potential adverse effects on the rectum such as chronic radiation-induced proctitis and fibrosis, which are characterized by multiplex symptoms (e.g., diarrhea, tenesmus, and rectal bleeding) and lead to significant challenges to patients [24]. Notably, individuals subjected to radiation in the pelvic region face an elevated risk of complications, including bowel obstruction or fistula formation, owing to fibrosis and compromised vascularity [25]. RICF represents a considerable health concern, contributing to mortality in occidental countries. Despite therapeutic interventions being predominantly palliative, the growing number of patients grappling with fibrosis underscores the pressing need for innovative approaches. Notably, in this study, we put forward the feasibility of continuous injection of UC-MSCs and AD-MSCs for alleviating the aforementioned complications in colorectal carcinoma (CRC) and RICF caused by radiotherapy.

Since the first identification in the 1960s, MSCs have been generated from diverse origins, including the adult tissue (e.g., bone marrow, dental pulp, adipose tissue) [12, 26, 27], perinatal tissue (e.g., umbilical cord, placenta, amniotic membrane and amniotic fluid) [10, 28, 29], and even stem cells (e.g., embryonic stem cells, induced pluripotent stem cells) [9, 11]. MSCs have been proved with splendid therapeutic effect upon diverse refractory and recurrent diseases (e.g., COVID-19 pneumonia, acute myeloid leukemia, acute-on-chronic liver failure) via paracrine and autocrine, trans- or direct-differentiation, anti-fibrosis, and bidirectional immunomodulation [12, 30, 31]. In this context, MSCs emerge as promising candidates, exhibiting diverse anti-fibrotic effects in both preclinical models and clinical practice [23, 32]. Leveraging their regenerative and anti-inflammatory properties, MSCs have demonstrated efficacy in treating conditions such as graft-versus-host disease (GvHD) [33] and radiation-induced burns [34]. Moreover, comprehensive investigations into the differences and similarities among MSCs prepared from diverse sources contribute valuable insights to their therapeutic potential [35, 36]. For instance, Zhang *et al* and Zhao *et al* respectively reported the variations in the outcomes of acute liver failure in rat (aLF) and acute GvHD (aGvHD) by UC-MSCs at various passages, which indicated the variations in the outcomes due to the otherness of MSC sources [10, 37]. In this study, we verified the consistency in therapeutic effect and variations in transcriptomic signatures upon RICF rats by continuous AD-MSC and UC-MSC treatment, which would benefit the further development of MSC-based cytotherapy with the two distinct cell sources.

As to RICF treatment, our data indicated the comparable anti-fibrotic effects of AD-MSCs and UC-MSCs according to multidimensional histological and transcriptomic analyses, including a substantial suppression in collagen content and proinflammatory factors. However, the detailed information of the representative DEGs in mediating the alleviative effect of both AD-MSCs and UC-MSCs upon RICF is largely undiscovered. Meanwhile, microvesicles of diverse particle size including exosomes (containing miRNAs, ceRNAs, cytokines, anti-fibrotic factors, etc) have been identified to play a pivotal role in mediating the efficacy of MSCs upon inflammatory diseases and fibrosis [38, 39]. Thus, it would be of great interesting to further illuminate the candidate DEGs and the network in orchestrating the anti-inflammatory and anti-fibrotic effect of AD-MSCs and UC-MSCs in future. For instance, the *in vitro* further verifica-

tion and further exploration of the DEGs enriched by RNA-seq bioinformatic analysis would be of great help for illuminating the potential roles of AD-MSCs and UC-MSCs upon RICF. Collectively, these findings underscore the potential therapeutic efficacy of MSCs, offering a glimpse into their ability to mitigate the deleterious effects of radiation-induced colorectal fibrosis. The comparative evaluation of AD-MSCs and UC-MSCs contributes novel insights into their respective anti-fibrotic and anti-inflammatory capability, supplying overwhelming new references for future investigations of MSC-based regimens for potential clinical applications in future.

Conclusions

Overall, our data verified the comparable remission of RICF rats after consecutive intraperitoneal infusion of two distinct MSCs including AD-MSCs and UC-MSCs. Furthermore, RICF rats with AD-MSC and UC-MSC treatment showed multifaceted conservations and alterations in gene expression pattern and genetic variations, which indicated the differences in the impact of transcriptomic signatures of colorectal tissue. Collectively, our findings would benefit the further assessment and development of MSC-based cytotherapy in preclinical and clinical investigations.

Acknowledgements

We thank Zhihong Huang, Junjin Lin, Suping Zheng and Ling Lin from the Public Technology Service Center (Fujian Medical University, Fuzhou, China) for their technical support. This study was supported by Natural Science Foundation of Fujian Province (2022J01753, 2022J01726), Joint Funds for the innovation of science and Technology of Fujian province (2019Y92050173), Fujian Provincial Health Technology Project (2020GGB022), the National Natural Science Foundation (82260031), project funded by China Postdoctoral Science Foundation (2023M730723), Postdoctoral Program of Natural Science Foundation of Gansu Province (23JRRA1319), Natural Science Foundation of Jiangxi Province (20224BAB206077), Gansu Provincial Hospital Intra-Hospital Research Fund Project (22GSSYB-6), and the 2022 Master/Doctor/Postdoctoral program of NHC Key Laboratory of Diagnosis and Therapy of Gastrointestinal Tumor (NHCDP2022004, NHCDP2022008).

Disclosure of conflict of interest

None.

Abbreviations

CRC, colorectal cancer; hAD-MSCs, human adipose-derived mesenchymal stem cells; hUC-MSCs, human umbilical cord-derived mesenchymal stem/stromal cells; RICF, radiation-induced colorectal fibrosis; RNA-SEQ, RNA-sequencing; MSCs, mesenchymal stem/stromal cells; RIS, radiation injury score; IHC, immunohistochemistry; IF, immunofluorescence; SD, Sprague-Dawley; GOBP, gene ontology biological process; VSEs, variable shear events; DVSEs, differentially VSEs; PPI, protein-protein interaction; PCA, principal component analysis; TPM, transcripts per kilobase million; FPKM, fragments per kilobase million; DEGs, differently expressed genes; GSEA, gene set enrichment analysis; KDA, key drive gene analysis.

Address correspondence to: Dr. Pan Chi and Shenghui Huang, Department of Colorectal Surgery, Fujian Medical University Union Hospital, No. 29, Xin Quan Road, Gulou District, Fuzhou 350001, Fujian, China. Tel: 0591-86218015; ORCID: 0000-0003-1343-3801; E-mail: chipan99@163.com (PC); ORCID: 0000-0003-2817-4902; E-mail: shepherd819@fjmu.edu.cn (SHH); Leisheng Zhang, Science and Technology Innovation Center, The Fourth People's Hospital of Jinan (The Third Affiliated Hospital of Shandong First Medical University), Jinan 250031, China. ORCID: 0000-0001-6540-0943; E-mail: leisheng_zhang@163.com

References

[1] Sun YW, Zhang YY, Ke XJ, Wu XJ, Chen ZF and Chi P. Pirfenidone prevents radiation-induced intestinal fibrosis in rats by inhibiting fibroblast proliferation and differentiation and suppressing the TGF-β1/Smad/CTGF signaling pathway. Eur J Pharmacol 2018; 822: 199-206.

[2] Huang S, Wang X, Sun Y, Lu X, Jiang W, Chen Z, Huang Y and Chi P. TMT-labelled quantitative proteomic analysis to identify the proteins underlying radiation-induced colorectal fibrosis in rats. J Proteomics 2020; 223: 103801.

[3] Sun W, Dou R, Chen J, Lai S, Zhang C, Ruan L, Kang L, Deng Y, Lan P, Wang L and Wang J. Impact of long-course neoadjuvant radiation on postoperative low anterior resection syndrome and quality of life in rectal cancer: post hoc analysis of a randomized controlled trial. Ann Surg Oncol 2019; 26: 746-755.

[4] Qin Q, Ma T, Deng Y, Zheng J, Zhou Z, Wang H, Wang L and Wang J. Impact of preoperative radiotherapy on anastomotic leakage and stenosis after rectal cancer resection: post hoc analysis of a randomized controlled trial. Dis Colon Rectum 2016; 59: 934-942.

[5] Kim CW, Kim JH, Yu CS, Shin US, Park JS, Jung KY, Kim TW, Yoon SN, Lim SB and Kim JC. Complications after sphincter-saving resection in rectal cancer patients according to whether chemoradiotherapy is performed before or after surgery. Int J Radiat Oncol Biol Phys 2010; 78: 156-163.

[6] Stacey R and Green JT. Radiation-induced small bowel disease: latest developments and clinical guidance. Ther Adv Chronic Dis 2014; 5: 15-29.

[7] Hamama S, Delanian S, Monceau V and Vozenin MC. Therapeutic management of intestinal fibrosis induced by radiation therapy: from molecular profiling to new intervention strategies et vice et versa. Fibrogenesis Tissue Repair 2012; 5 Suppl 1: S13.

[8] Wu Q, Zhang L, Su P, Lei X, Liu X, Wang H, Lu L, Bai Y, Xiong T, Li D, Zhu Z, Duan E, Jiang E, Feng S, Han M, Xu Y, Wang F and Zhou J. MSX2 mediates entry of human pluripotent stem cells into mesendoderm by simultaneously suppressing SOX2 and activating NODAL signaling. Cell Res 2015; 25: 1314-1332.

[9] Zhang L, Wang H, Liu C, Wu Q, Su P, Wu D, Guo J, Zhou W, Xu Y, Shi L and Zhou J. MSX2 Initiates and accelerates mesenchymal stem/stromal cell specification of hPSCs by regulating TWIST1 and PRAME. Stem Cell Reports 2018; 11: 497-513.

[10] Zhao Q, Zhang L, Wei Y, Yu H, Zou L, Huo J, Yang H, Song B, Wei T, Wu D, Zhang W, Zhang L, Liu D, Li Z, Chi Y, Han Z and Han Z. Systematic comparison of hUC-MSCs at various passages reveals the variations of signatures and therapeutic effect on acute graft-versus-host disease. Stem Cell Res Ther 2019; 10: 354.

[11] Zhang L, Wei Y, Chi Y, Liu D, Yang S, Han Z and Li Z. Two-step generation of mesenchymal stem/stromal cells from human pluripotent stem cells with reinforced efficacy upon osteoarthritis rabbits by HA hydrogel. Cell Biosci 2021; 11: 6.

[12] Zhang L, Chi Y, Wei Y, Zhang W, Wang F, Zhang L, Zou L, Song B, Zhao X and Han Z. Bone marrow-derived mesenchymal stem/stromal cells in patients with acute myeloid leukemia reveal transcriptome alterations and deficiency in cellular vitality. Stem Cell Res Ther 2021; 12: 365.

[13] Fraser JK, Wulur I, Alfonso Z and Hedrick MH. Fat tissue: an underappreciated source of stem cells for biotechnology. Trends Biotechnol 2006; 24: 150-154.

[14] Vieira NM, Brandalise V, Zucconi E, Secco M, Strauss BE and Zatz M. Isolation, characterization, and differentiation potential of canine adipose-derived stem cells. Cell Transplant 2010; 19: 279-289.

[15] Zhang H, Zhang B, Tao Y, Cheng M, Hu J, Xu M and Chen H. Isolation and characterization of mesenchymal stem cells from whole human umbilical cord applying a single enzyme approach. Cell Biochem Funct 2012; 30: 643-649.

[16] Capelli C, Gotti E, Morigi M, Rota C, Weng L, Dazzi F, Spinelli O, Cazzaniga G, Trezzi R, Gianatti A, Rambaldi A, Golay J and Introna M. Minimally manipulated whole human umbilical cord is a rich source of clinical-grade human mesenchymal stromal cells expanded in human platelet lysate. Cytotherapy 2011; 13: 786-801.

[17] Marmotti A, Mattia S, Bruzzone M, Buttiglieri S, Risso A, Bonasia DE, Blonna D, Castoldi F, Rossi R, Zanini C, Ercole E, Defabiani E, Tarella C and Peretti GM. Minced umbilical cord fragments as a source of cells for orthopaedic tissue engineering: an in vitro study. Stem Cells Int 2012; 2012: 326813.

[18] El Omar R, Beroud J, Stoltz JF, Menu P, Velot E and Decot V. Umbilical cord mesenchymal stem cells: the new gold standard for mesenchymal stem cell-based therapies? Tissue Eng Part B Rev 2014; 20: 523-544.

[19] Abraham D and Distler O. How does endothelial cell injury start? The role of endothelin in systemic sclerosis. Arthritis Res Ther 2007; 9 Suppl 2: S2.

[20] Pu X, Zhang L, Zhang P, Xu Y, Wang J, Zhao X, Dai Z, Zhou H, Zhao S and Fan A. Human UC-MSC-derived exosomes facilitate ovarian renovation in rats with chemotherapy-induced premature ovarian insufficiency. Front Endocrinol (Lausanne) 2023; 14: 1205901.

[21] Wei Y, Hou H, Zhang L, Zhao N, Li C, Huo J, Liu Y, Zhang W, Li Z, Liu D, Han Z, Zhang L, Song B, Chi Y and Han Z. JNKi- and DAC-programmed mesenchymal stem/stromal cells from hESCs facilitate hematopoiesis and alleviate hind limb ischemia. Stem Cell Res Ther 2019; 10: 186.

[22] Wei Y, Zhang L, Chi Y, Ren X, Gao Y, Song B, Li C, Han Z, Zhang L and Han Z. High-efficient generation of VCAM-1(+) mesenchymal stem cells with multidimensional superiorities in signatures and efficacy on aplastic anaemia mice. Cell Prolif 2020; 53: e12862.

[23] Huo J, Zhang L, Ren X, Li C, Li X, Dong P, Zheng X, Huang J, Shao Y, Ge M, Zhang J, Wang M, Nie N, Jin P and Zheng Y. Multifaceted characterization of the signatures and efficacy of mesenchymal stem/stromal cells in acquired aplastic anemia. Stem Cell Res Ther 2020; 11: 59.

[24] Ashcraft KA, Miles D, Sunday ME, Choudhury KR, Young KH, Palmer GM, Patel P, Woska EC, Zhang R, Oldham M, Dewhirst MW and Koontz BF. Development and preliminary evaluation of a murine model of chronic radiation-induced proctitis. Int J Radiat Oncol Biol Phys 2018; 101: 1194-1201.
[25] Usunier B, Brossard C, L'Homme B, Linard C, Benderitter M, Milliat F and Chapel A. HGF and TSG-6 released by mesenchymal stem cells attenuate colon radiation-induced fibrosis. Int J Mol Sci 2021; 22: 1790.
[26] Wang L, Zhang L, Liang X, Zou J, Liu N, Liu T, Wang G, Ding X, Liu Y, Zhang B, Liang R and Wang S. Adipose tissue-derived stem cells from type 2 diabetics reveal conservative alterations in multidimensional characteristics. Int J Stem Cells 2020; 13: 268-278.
[27] Ning J, Zhang L, Xie H, Chai L and Yao J. Decoding the multifaceted signatures and transcriptomic characteristics of stem cells derived from apical papilla and dental pulp of human supernumerary teeth. Cell Biol Int 2023; 47: 1976-1986.
[28] Hou H, Zhang L, Duan L, Liu Y, Han Z, Li Z and Cao X. Spatio-temporal metabolokinetics and efficacy of human placenta-derived mesenchymal stem/stromal cells on mice with refractory crohn's-like enterocutaneous fistula. Stem Cell Rev Rep 2020; 16: 1292-1304.
[29] Sun Y, Wang TE, Hu Q, Zhang W, Zeng Y, Lai X, Zhang L and Shi M. Systematic comparation of the biological and transcriptomic landscapes of human amniotic mesenchymal stem cells under serum-containing and serum-free conditions. Stem Cell Res Ther 2022; 13: 490.
[30] Zhang LS, Yu Y, Yu H and Han ZC. Therapeutic prospects of mesenchymal stem/stromal cells in COVID-19 associated pulmonary diseases: from bench to bedside. World J Stem Cells 2021; 13: 1058-1071.
[31] Nevens F and van der Merwe S. Mesenchymal stem cell transplantation in liver diseases. Semin Liver Dis 2022; 42: 283-292.
[32] Yu H, Feng Y, Du W, Zhao M, Jia H, Wei Z, Yan S, Han Z, Zhang L, Li Z and Han Z. Off-the-shelf GMP-grade UC-MSCs as therapeutic drugs for the amelioration of CCl4-induced acute-on-chronic liver failure in NOD-SCID mice. Int Immunopharmacol 2022; 113: 109408.
[33] Munneke JM, Spruit MJ, Cornelissen AS, van Hoeven V, Voermans C and Hazenberg MD. The potential of mesenchymal stromal cells as treatment for severe steroid-refractory acute graft-versus-host disease: a critical review of the literature. Transplantation 2016; 100: 2309-2314.
[34] Tamarat R, Lataillade JJ, Bey E, Gourmelon P and Benderitter M. Stem cell therapy: from bench to bedside. Radiat Prot Dosimetry 2012; 151: 633-639.
[35] Chamberlain G, Fox J, Ashton B and Middleton J. Concise review: mesenchymal stem cells: their phenotype, differentiation capacity, immunological features, and potential for homing. Stem Cells 2007; 25: 2739-2749.
[36] Qi Z, Zhang Y, Liu L, Guo X, Qin J and Cui G. Mesenchymal stem cells derived from different origins have unique sensitivities to different chemotherapeutic agents. Cell Biol Int 2012; 36: 857-862.
[37] Zhang Y, Li Y, Li W, Cai J, Yue M, Jiang L, Xu R, Zhang L, Li J and Zhu C. Therapeutic effect of human umbilical cord mesenchymal stem cells at various passages on acute liver failure in rats. Stem Cells Int 2018; 2018: 7159465.
[38] Shen Z, Huang W, Liu J, Tian J, Wang S and Rui K. Effects of mesenchymal stem cell-derived exosomes on autoimmune diseases. Front Immunol 2021; 12: 749192.
[39] Lin Z, Wu Y, Xu Y, Li G, Li Z and Liu T. Mesenchymal stem cell-derived exosomes in cancer therapy resistance: recent advances and therapeutic potential. Mol Cancer 2022; 21: 179.

Table S1. Antibodies for immunohistochemistry (IHC) analysis

Antibody	Cat. NO.	Source	Concentration
Anti-rabbit-collagen 1	AF7001	Affinity Biosciences	1:200
Anti-rabbit-α-smooth muscle actin	ab124964	Abcam	1:1000
Anti-rabbit-fibronectin	ab2413	Abcam	1:250
Goat anti-rabbit IgG H&L/Biotin	bs-0295G-Bio	Bioss	1:200
Streptavidin/HRP	bs-0437P-HRP	Bioss	1:1000

Table S2. Antibodies for immunofluorescence (IF) analysis

Antibody	Cat. NO.	Source	Concentration
Anti-mouse-collagen 1	66761-1-Ig	Proteintech	1:200
Anti-rabbit-fibronectin	ab2413	Abcam	1:200
Goat anti-rabbit IgG H&L/Alexa Fluor FITC	bs-0295G-FITC	Bioss	1:200
Goat anti-mouse IgG H&L/Alexa Fluor 594-labelled	bs-0296G-AF594	Bioss	1:200

Table S3. Primer sequences of candidate genes for qRT-PCR analysis

Gene	Forward Primer	Reverse Primer
α-SMA	ACCATCGGGAATGAACGCTT	CTGTCAGCAATGCCTGGGTA
TGF-β1	CAACAATTCCTGGCGTTACCT	TGTATTCCGTCTCCTTGGTTCA
Collagen-1	CGAGTATGGAAGCGAAGGTT	CTTGAGGTTGCCAGTCTGTT
Collagen-3	GCCTCCCAGAACATTACATACC	CTTGCTCCATTCACCAGTGT
SERPINE-1	AGCTGGGCATGACTGACATC	TGCGGGCTGAGACTAGAATG
TIMP-1	TTCCTGGTTCCCTGGCATAA	ATCTGATCTGTCCACAAGCAATG
Fibronectin	ACCAAGTATGAAGTCAGCGTCTA	GGAAGCCAGTGATCGTCTCT
GAPDH	ACGGCAAGTTCAACGGCACAG	GAAGACGCCAGTAGACTCCACGAC
IL-1β	GCTACCTATGTCTTGCCCGT	TCACACACTAGCAGGTCGTC
IL-6	GACTTCCAGCCAGTTGCCTT	CTGGTCTGTTGTGGGTGGTAT

Table S4. Antibodies for western blot analysis

Antibody	Cat. NO.	Source	Concentration
Anti-rabbit-collagen 1	AF7001	Affinity Biosciences	1:1000
Anti-rabbit-α-smooth muscle actin	ab124964	Abcam	1:50000
Anti-rabbit-fibronectin	ab2413	Abcam	1:2000
anti-rabbit-CTGF	bs-0743R	Bioss	1:1000
anti-mouse-TGF-β1	bsm-33345M	Bioss	1:5000
anti-rabbit-SMAD2+SMAD3 (phosphoT8)	ab272332	Abcam	1:1000
anti-mouse-Vimentin	60330-1-Ig	Proteintech	1:20000
anti-rabbit-MMP-2	ab92536	Abcam	1:2000
anti-rabbit-MMP-9	10375-2-AP	Proteintech	1:500
anti-mouse-GAPDH	60004-1-Ig	Proteintech	1:50000
Peroxidase-conjugated Affinipure Goat Anti-Rabbit IgG(H+L)	SA00001-2	Proteintech	1:2000
HRP-conjugated Peroxidase-conjugated Affinipure Goat Anti-Mouse IgG(H+L)	SA00001-1	Proteintech	1:2000